Environmental Science and Ecotechnology 11 (2022) 100181

Contents lists available at ScienceDirect

Environmental Science and Ecotechnology

journal homepage: www.journals.elsevier.com/environmental-science-and-ecotechnology/

Original Research

Reduction, mineralization, and magnetic removal of chromium from soil by using a natural mineral composite

Xiang Ji [a], Chuanye Zhou [a], Liangxi Chen [a], Yanzhang Li [a], Tianci Hua [a], Yan Li [a], Changqiu Wang [a], Song Jin [b, c], Hongrui Ding [a, **], Anhuai Lu [a, *]

[a] Beijing Key Laboratory of Mineral Environmental Function, School of Earth and Space Sciences, Peking University, Beijing, 100871, China
[b] Advanced Environmental Technologies LLC, 4025 Automation Way, Unit F4, Fort Collins, CO, 80525, USA
[c] Department of Civil and Architectural Engineering, University of Wyoming, Laramie, WY, 82071, USA

ARTICLE INFO

Article history:
Received 16 February 2022
Received in revised form
2 April 2022
Accepted 3 April 2022

Keywords:
Cr
Magnetic
Mineral composite
Mineralization
Soil remediation

ABSTRACT

Reductive immobilization has been a commonly used technique to detoxify Cr(VI) from soil; however, it's challenging to remove the reduced Cr from soil to prevent its re-oxidation. This work explored a natural magnetic composite for the remediation, mineralization, and magnetic removal of Cr(VI) from the soil. It consists of 77% magnetite and 23% pyrrhotite with strong magnetic properties. A series of characterization tests show that composites of magnetite and pyrrhotite are interlaced and closely bonded, and contain no other heavy metals. The Cr(VI) removal rate increases with the decrease in composite particle size. A kinetics study shows that removing Cr(VI) by the composite is likely through both adsorption and reduction. Acidic conditions are more favorable for the immobilization of Cr(VI), at 45.8 mg Cr(VI) removal per g of composite at pH 2. After 100 days of *in-situ* treatment by the composite, the leaching concentration (TCLP) of Cr(VI)-contaminated soil was 1.95 mg L^{-1}, which was below the EPA limit (5 mg L^{-1}) for hazardous waste. After reduction, the composite was separated from soil by magnetic characteristics, and 58.2% of Cr was found mineralized. The post-treatment Cr-containing composite was analyzed by SEM-EDS, Raman spectra, and XPS. It was found that Cr was mineralized on the surface of the composite in the form of $Cr(OH)_3$, Cr_2O_3, and $FeCr_2O_4$. This indicates that reduction and mineralization of Cr(VI) in the soil can be accomplished through natural magnetic mineral composites and easily separated and removed from the soil, achieving a complete soil cleanup.

1. Introduction

Cr is widely used in industrial applications, such as leather tanning, electroplating, wood preservation, printing, and dyeing [1]. A large amount of Cr slag is produced as a result of these processes, and along with the leaching of rain, releases copious amounts of Cr into soil and groundwater [2–6]. The most common states of Cr are Cr(III) and Cr(VI), which are present in the natural environment. In basic solutions above pH = 6, Cr(VI) forms the tetrahedral yellow chromate ion CrO_4^{2-}; between pH 2 and 6, CrO_4^{2-} and the orange-red dichromate ion $Cr_2O_7^{2-}$ are in equilibrium [7]. In general, Cr(VI) compounds are more toxic than Cr(III) compounds. This is attributed to the stronger oxidizing power and the higher membrane transport of the former chemical compound [8]. Tissue damage, irritative lesions of the skin and respiratory tract, and cell-mediated allergic reactions caused by exposure to Cr(VI) are well documented [9–11]. Due to its serious threat to the human body and environment, the World Health Organization (WHO) recommends the maximum allowable contaminant level to be 0.05 mg L^{-1} of Cr(VI) in drinking water [12]. Unlike Cr(VI), Cr(III) is relatively stable in the environment and is considered an essential element for human and plant nutrition [13,14]. Therefore, reducing Cr(VI) to Cr(III) is usually a key mechanism to remediate Cr-contaminated soil.

Traditional techniques are applied to remediate contaminated soil, including chemical reductions [15], electrokinetic processes [16], soil washing [17], and phytoremediation [18]. In recent years, *in situ* remediation of Cr-contaminated soil by delivering reactive materials into the soil has been considered a promising technology.

* Corresponding author.
** Corresponding author.
E-mail addresses: dhr@pku.edu.cn (H. Ding), ahlu@pku.edu.cn (A. Lu).

https://doi.org/10.1016/j.ese.2022.100181

Materials such as biochar, nZVI, nano-FeS_2, nano-$MnFe_2O_4$, nano-Fe_3O_4, and their composites are widely studied for this process [19–27]. However, these synthetic nanomaterials usually have relatively high costs and toxicity [28–30]. Other low-cost and eco-friendly materials are necessary to reduce and immobilize Cr(VI) in contaminated soils. If Cr(VI) remains in the soil after reduction, it can be easily re-oxidized; however, complete reduction and mineralization of Cr(VI) to separate it from the soil remains a difficult problem.

Pyrrhotite is a common natural iron sulfide and shows a non-stoichiometric composition as $Fe_{1-x}S$, where x varies from 0 (FeS) to 0.125 (Fe_7S_8) [31]. Fe^{2+} and S^{2-} in the lattice are electron donors, making pyrrhotite a rare reducing agent in nature [32]. Previous studies have shown that natural pyrrhotite can effectively remove Cr(VI) from aqueous solutions [33,34]. However, natural iron sulfide usually contains a variety of heavy metals; as a result, there are few studies on its application in soil remediation. Magnetite is widely distributed in soils and sediments [35,36]. It has been proven that magnetite possesses certain adsorption and removal capacities for Cr(VI) in various solutions [37,38]. Additionally, magnetite is frequently used as a magnetic carrier to facilitate the recovery of materials after remediation [39–41]. Given that these two minerals are commonly associated in nature and can remove Cr(VI), their composite is likely to be a low-cost and eco-friendly material for remediation of Cr-contaminated soil.

The main objectives of the study are to investigate the effectiveness of natural magnetic mineral composites (pyrrhotite and magnetite) to immobilize Cr in soil. Thus, the characterizations of the composite are studied, and the capability of the composite to reduce Cr(VI) is examined by a series of solution experiments and *in-situ* soil remediation tests. We used the magnetic characteristics of the composite to separate Cr from the soil and analyze its phase to showcase the mineralization of Cr(VI) by the natural pyrrhotite/magnetite composites.

2. Materials and methods

2.1. Materials

The natural magnetic mineral composite (pyrrhotite/magnetite) was obtained from an iron mine in Shanxi, China, and crushed in the laboratory. The Cr(VI)-simulated solution was prepared in the laboratory by using potassium dichromate (K_2CrO_7, 99%) with an initial concentration of 100 mg L^{-1}. Other Cr(VI) solutions with different initial concentrations were made through dilution. pH was adjusted by adding dilute hydrochloric acid (HCl, 3%) or sodium hydroxide (NaOH, 1%) solution. Cr(VI)-contaminated soil used in the *in-situ* remediation tests was prepared in the laboratory. Cr-free soil was collected from Hunan, China. Cr(VI)-contaminated soil was prepared by mixing 0.5 L of $K_2Cr_2O_7$ solution with 1 kg of air-dried soil. This was stirred thoroughly until the mixture was air-dried to a constant weight: the resulting Cr(VI) concentration was 500 mg kg^{-1} [42]. The soil was completely dried and sterilized for use in subsequent experiments. All the chemicals used in this study were analytical and purchased from Sinopharm Chemical Reagent Co., Ltd.

2.2. Batch experiments

The mineral composites with different particle sizes (>270 μm; 150–270 μm; 75–150 μm; and 48–75 μm) were added into 50 mL simulated solutions of 100 mg L^{-1} Cr(VI) to study the effect of particle sizes on Cr(VI) reduction. The adsorption kinetics were analyzed by pseudo-first-order and pseudo-second-order models, respectively. Another set of experiments was performed by adding 1 g L^{-1} mineral composites into solutions with different initial pH to find out the influence of pH value on the saturated reduction capacity of the composites. Deionized and deoxygenated (dissolved oxygen < 0.3 mg L^{-1}) water was prepared and used throughout the experiment [43]. All Cr(VI) removal reactions were carried out in the 100 mL H_2SO_4-cleaned conical flask and conducted in triplicates.

2.3. In-situ soil remediation tests

In order to simulate the *in-situ* remediation effect of Cr(VI) in the soil by the magnetic mineral composites, different qualities of the mineral composite (5, 10, 15, and 20 wt%) with the particle size of 48–75 μm were mixed with the prepared Cr(VI)-contaminated soil [42]. Deionized water was used to adjust the water content of soil (10%, 20%, 30%, 40%. and 50%) to simulate the effects of different water conditions on *in-situ* remediation of Cr(VI). During the experiment, the sealing film was used to seal the soil system to maintain water content and eliminate the influence of atmospheric oxidation. All experiments lasted 100 days and were conducted in triplicates. After conducting the reactions, both the control and experimental soil were completely dried. A group of soil with a 50% water ratio was used as an external magnetic field to separate the magnetic minerals from the soil. The Cr content of separated magnetic minerals and soil was analyzed to study the distribution of Cr(VI), and a series of analyses were performed to verify the mineralization of Cr(VI) in the soil.

2.4. Chemical stability of Cr in the soil

Toxicity characteristic leaching procedure (TCLP) has been widely applied to assess the effectiveness of toxic metals immobilization procedures in contaminated soil [22,44–46]. The method is conducted as follows: air-dried soil samples were extracted with the TCLP fluid (5.7 mL of glacial acetic acid in deionized water, diluted to 1 L, and maintained pH of the solution at 2.88 ± 0.05) for 18 h at a solid-to-solution ratio of 1 g–20 mL on a rotating shaker at room temperature (21 ± 1 °C) [47]. Cr(VI) concentration in the TCLP fluid and the simulation solutions was measured at 540 nm with a UV–visible spectrophotometer (Thermo Fisher EVOLUTION 220) using a diphenylcarbazide reagent. The un-leachable Cr(VI) in the soil was tested after digestion with an inductively coupled plasma atomic emission spectrometer (Spectro BLUE SOP) in accordance with the method HJ 491-2019 of China.

2.5. Analytical methods

The pH value was measured by a pH meter (Metler Toledo EL20) with a combined glass electrode. A vibrating sample magnetometer (Agico MFK1-FA) was used to analyze the magnetic properties of the samples at 300 K. The surface morphology test of samples was observed on the field emission environmental scanning electron microscopy (Thermo Fisher Quattro ESEM). Courtesy of the school of physics at Peking University, elemental composition analysis was completed with an accompanying X-ray energy spectrometer. XRD analysis of the composite was performed with an X-ray diffractometer (Philips X'PertPro) in the school of chemistry and molecular engineering at Peking University. Raman analysis was performed on a Laser-Raman micro-spectroscopy (Renishaw, inVia Reflex) at the school of earth and space sciences, Peking University, with a scanning range of 100–1400 cm^{-1}. XRF analysis was carried out on the X-ray fluorescence spectrometer (Thermo ARL ADVANT' XP+) at the school of earth and space sciences, Peking University. XPS analysis was completed on the X-ray photoelectron spectroscopy (Kratos AXIS Supra) at Peking University.

3. Results and discussion

3.1. Characterization of the natural magnetic composite

Natural ores were collected from mines and broken in the laboratory. The composites were obtained through a simple magnetic separation. The crystal structures of the samples were investigated by an X-ray diffractometer. As shown in Fig. 1a, the samples have sharp diffraction peaks, indicating a high degree of crystallization of the natural minerals. Diffraction peaks of the composite can be indexed as two minerals, pyrrhotite and magnetite. Typical diffraction peaks such as (110), (−221), and (402) crystal planes at $2\theta = 15.3°$, 29.9°, and 43.7°, respectively, indicate that the mineral is pyrrhotite (PDF#52-1516). Diffraction peaks at $2\theta = 30.1°$, 35.4°, and 62.5° correspond to (220), (311), and (440) crystal planes of magnetite (PDF#11-0614). Since there are no peaks of other mineral phases in the XRD pattern, a semi-quantitative analysis can be carried out by RIR value. The two minerals account for 77% magnetite and 23% pyrrhotite in the composite.

Both magnetite and pyrrhotite particles demonstrate the presence of a ferromagnetic state [48,49]. Fig. 1b displays the magnetic hysteresis loop of the natural mineral composites at room temperature. The saturation magnetization value (Ms) of the composite in this paper is approximately 68 emu g^{-1}, the values of coercivity (Hc) is about 0.25k Oe, and the remanence (Mr) is 8.7 emu g^{-1}, values which are lower than those of synthesized Fe_3O_4 nanoparticles [50] However, these values are significantly higher than natural pyrrhotite [49]. It should be noted that the magnetic characteristics of minerals are significantly affected by particle size [51]. Immobilized materials used in this study are composited of these two minerals, possessing the strong magnetism of magnetite and the high reactivity of pyrrhotite. Therefore, we can use the magnetic characteristics of the minerals and their composites to conduct magnetic separation of the treated soil and allow for subsequent research on the mineralization of Cr(VI).

The morphology of the natural composite was observed from the SEM images in Fig. 1c. After crushing and screening, the minerals have taken on an irregular shape. The particles have clear edges and are relatively smooth, but there is a small amount of debris adsorbed on the surface of the particle due to magnetic properties. Through *in-situ* X-ray energy spectrum mapping analysis, we found that the mineral particle is mainly composed of Fe, S, and O. It should be noted that Fe is evenly distributed on the mineral surface while O is interlaced with S. This indicates that iron oxide and iron sulfide in the mineral-composites are interlaced and closely bonded; reductive iron sulfide can be effectively exposed and involved in the reduction of Cr(VI) as well.

In-situ microscopic Raman analysis was performed on the labeled positions in Fig. 1c, with corresponding results shown in Fig. 1d. The position marked in pink shows three Raman peaks, located at 306, 538, and 665 cm^{-1}. This is consistent with the Raman peak positions of Fe_3O_4 reported in the previous study [52]. The shift of the peaks at 314, 360, and 379 cm^{-1} indicated pyrrhotite [53,54] and can be observed at positions that are marked yellow.

In general, natural iron sulfide has other heavy metals to replace the cations in the mineral crystal lattice, such as Pb, Zinc, etc. It will partially dissolve within reactions, which causes secondary pollution and limits the application of natural iron sulfide in pollution remediation. No other heavy metals were present on the surface of the mineral composites by EDS in Fig. 1c. In order to further verify the risk of secondary contamination of natural mineral composites, a total element analysis of the mineral was performed through XRF. According to Table 1, the highest concentration of the elements was Fe, O, S, Si, Ca, Na, Al, Mg, Mn, and Ti. Fe, O, and S concentrations in the mineral composites exceeded 95%, while the remaining elements were all less than 10 mg kg^{-1}. No other heavy metals (Pb, Cd, As) were found in the natural minerals used in this study.

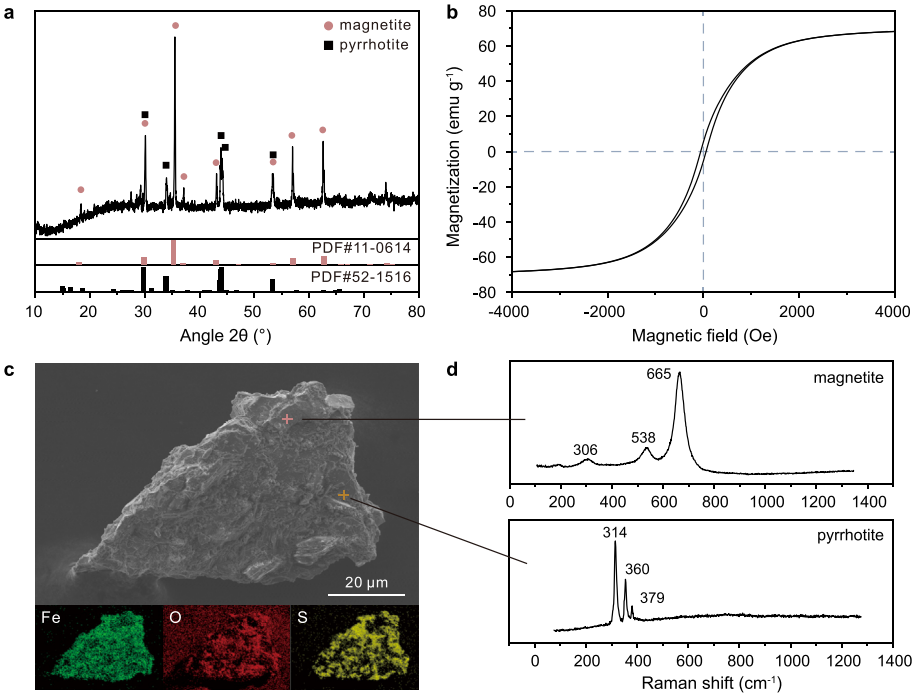

Fig. 1. **a**, XRD patterns of the natural minerals composite. **b**, Magnetic hysteresis loop of the composite. **c**, SEM images of the composites and element mapping of the particle. **d**, *in-situ* Raman analysis of the composite.

Table 1
The elemental composition of the minerals by XRF.

El	Fe	O	S	Si	Ca	Na	Al	Mg	Mn	Ti
Wt%	63.15	25.04	8.61	1.42	0.762	0.314	0.244	0.143	0.137	0.091
StdErr	0.15	0.12	0.12	0.04	0.037	0.017	0.007	0.007	0.004	0.004

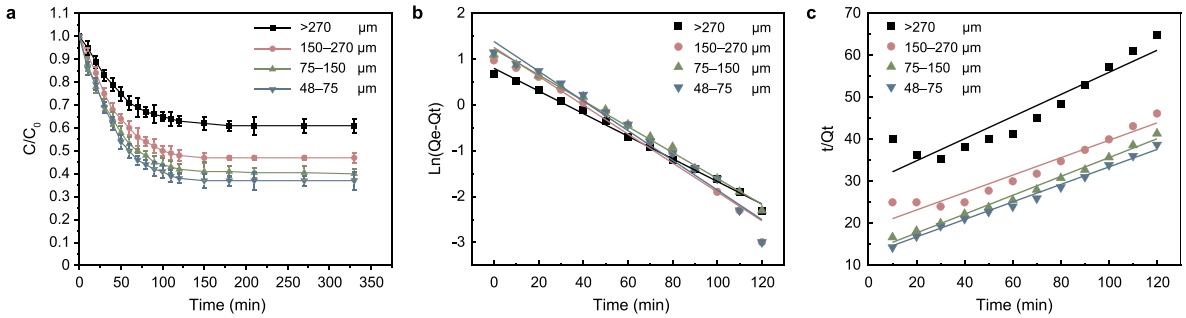

Fig. 2. **a**, Cr(VI) removal in solutions by different particle sizes of minerals. **b**, The pseudo-first-order kinetic fitting. **c**, The pseudo-second-order kinetic fitting.

3.2. Aqueous Cr(VI) removal

3.2.1. Influence of the particle size on the Cr(VI) removal

Parallel experiments were conducted to investigate the influence on the particle size of mineral composites in regards to Cr(VI) removal. As shown in Fig. 2a, the reduction of Cr(VI) pertaining to different mineral particle sizes can reach equilibrium within 150 min in solutions with pH 5.56. Moreover, the removal rate decreases with the increase of mineral particle size: with a mineral particle size larger than 270 μm, the removal rate of Cr(VI) was 39%; between 150 and 270 μm, the removal rate increased to 55%; and between 75–150 μm and 48–75 μm the remove rate was 60% and 62%, respectively. This indicates the influence of particle size on the removal rate of Cr(VI) is gradually weakened across a certain range due to limited exposure of the highly reactive pyrrhotite over a smaller surface area. As a result, it needs to be broken down into smaller particle sizes to ensure easier access and participation of pyrrhotite in Cr(VI) reduction.

Fig. 2b and c show the fitting results of the pseudo-first-order and the pseudo-second-order kinetic studies, respectively. Table 2 lists the corresponding parameters of kinetic equations. When the mineral particle size was larger than 270 μm, the removal process did not fit the pseudo-second-order kinetics model ($R^2 = 0.8724$) but lined up with pseudo-first-order kinetics with a higher coefficient of determination ($R^2 = 0.9942$) for the plots of t/Qt versus t. This indicates that the removal of Cr(VI) is conducted mainly by physical adsorption at this particular particle size. However, in relation to other particle sizes, the removal of Cr(VI) fits the model pseudo-second-order kinetics instead. The coefficient of determination R^2 of the pseudo-second-order equation increased from 0.9717 to 0.9987 when the particle size decreased from 150–270 μm to 48–75 μm. This means that with the decrease of particle size, Cr(VI) removal is more inclined to undergo chemisorption in correspondence to the exposed surface area of pyrrhotite. Furthermore, the increase of k_2 indicates that the adsorption rate will increase inversely with particle size. The decrease of particle size of mineral composite means the increase of specific surface area, and a larger specific surface area can absorb more Cr(VI), so the removal rate of Cr(VI) increases with the decrease of particle size [26,33].

3.2.2. Influence of the initial pH on Cr(VI) removal

At different pH values, the mineral composites were added to the Cr(VI) solutions, and the amount of Cr(VI) removal per gram of composite was calculated after balancing the reaction. According to the results in Fig. 3, the mineral composites exhibited higher reactivity for Cr(VI) removal under acidic conditions. The amount of Cr(VI) removal per gram of composite is 45.8 and 43.6 mg g^{-1} when the pH of the solution is 2 and 3, respectively. When the pH was raised to 4, the removal rate decreased significantly to 33.6 mg g^{-1} and continued on this trend with the further increase of pH value. At pH 9, the amount of Cr(VI) removal per gram was 24.1 mg g^{-1}. This effect of pH on the removal of Cr(VI) is the result of acidic conditions causing pyrrhotite ($pH_{pzc} = 2–3$) and magnetite ($pH_{pzc} = 6–7$) to adopt a positive charge on its surface, which is conducive to the adsorption of Cr(VI) anions [37,55]. Pyrrhotite will dissolve under acidic conditions (pH < 5) and release Fe^{2+} and S^{2-} ions [56], which can enhance reactional activity through direct electron transfer to Cr(VI). Therefore, when Cr(VI) solution is neutral and alkaline (pH 7–9), the adsorption and reduction rates of Cr(VI) are weak due to competition of OH^- with Cr(VI) on adsorption sites. This, along with precipitates such as $Fe(OH)_3$, will deposit on the surface and cause composites to lose reactivity rapidly [57].

Cr contaminated soils found in southern China are mostly acidic, with a pH range of 4–6 [58], which is conducive to using natural magnetic mineral composites as a form of soil remediation. The

Table 2
The parameters of the kinetic equations.

	The pseudo-first-order			The pseudo-second-order		
	Qe (mg g^{-1})	k_1 (min^{-1})	R^2	Qe (mg g^{-1})	k_2 (min^{-1})	R^2
>270 μm	19.44	0.024	0.9942	21.99	0.48	0.8724
150–270 μm	26.58	0.031	0.9306	27.15	1.22	0.9717
75–150 μm	31.21	0.032	0.9723	30.26	1.51	0.9896
48–75 μm	32.45	0.038	0.9618	31.52	1.83	0.9987

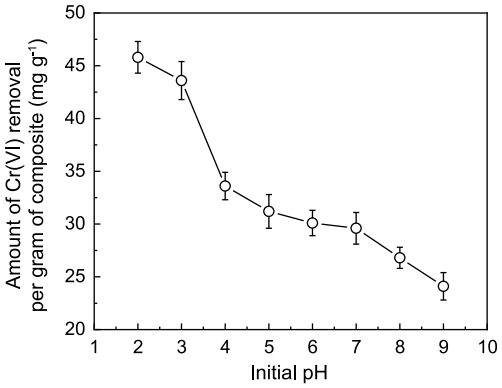

Fig. 3. Amount of Cr(VI) removal per gram of composite under different initial pHs.

main mineral components in soil are quartz and feldspar, and there are also some clay minerals. These minerals usually have a negative charge on the surface under acidic conditions [59,60], which is one of the reasons why the Cr(VI) anion is easy to migrate in soil. However, the mineral composite used in this paper has a positive charge on the surface at this pH value. When the Cr(VI) anion migrates with an aqueous solution in soil, it will be pre-adsorbed by the material and then reduced on the surface. Therefore, the moisture content in soil may be one of the main factors affecting the soil remediation by the composite. In the following, we carried out *in-situ* remediation experiments using Cr contaminated soil.

3.3. Reduction of Cr(VI) in the contaminated soil

3.3.1. The TCLP leachability of the Cr(VI) contaminated soil after remediation

In order to test the *in-situ* effects of treatments of Cr(VI)-contaminated soil in natural environments, the immobilization efficiency of the composites was measured. The soil used in this experiment was collected from Hunan Province, China, with a pH value of 4.02 and an average water ratio of 29.23%. To remove the influence of microorganisms on the reduction process of Cr(VI), the soil was sterilized before experimenting. Fig. 4 illustrates the TCLP leachability of Cr(VI) in treated and untreated soil under different conditions over 100 days. The highest leachability of Cr(VI), with an extraction rate of 69.8%, was observed in untreated soil with 0% water content. In the control group (no mineral composites in soil), leachable Cr(VI) concentration decreased slightly as the water ratio increased after 100 days of deposits. This may be due to the ability of clay minerals in the soil to immobilize Cr in the presence of water. As a result, when mineral composites were added to the contaminated soil, the leaching capacity of Cr(VI) decreased after 100 days of *in-situ* remediation. This indicates that adding natural mineral composites to the contaminated soil can effectively reduce Cr(VI) in soil, and subsequently the leaching risk of Cr. This trend becomes more significant with the increase in mineral dosage. In the experimental group with 30% water content, the TCLP-leachability of Cr(VI) was reduced to 49.6% when the mineral dosage was 10% and 29.1% when the mineral dosage was increased to 20%. However, we found that when the soil was completely dry (0% water ratio), the treatment group supplemented with 20% mineral material did not prominently reduce Cr(VI). Soil moisture is one of the key parameters in heavy metal contaminated soil remediation that will influence efficiency [4]. The Cr(VI) TCLP leachability of the composites-treated soil with the variation of soil moisture was investigated. The extraction rate of Cr(VI) was 60.3%, 56.1%, 49.6%, 29.6%, and 22.6% at a different soil moisture levels of 10%, 20%, 30%, 40%, and 50%, respectively, with the addition of 10% mineral composites. An increase in soil moisture corresponds to significant decreases in the leaching rate of Cr(VI). Leaching rates were 35.1%, 22.6%, 10.7%, and 7.8% when the soil moisture level increased to 50% at different dosages (5%, 10%, 15%, and 20%) of mineral composites. At a 20% mineral dosage, the leaching concentration was 1.95 mg L^{-1} after 100 days of treatment at a soil moisture level of 50%; this was below the EPA TCLP limit (5 mg L^{-1}) for hazardous waste (USEPA Method 1311, 1990). The increase of water content improves the migration and transformation of Cr in soil, conducive to the pre-adsorption of Cr(VI) by mineral composites and reduction by pyrrhotite. Therefore, the soil remediation process of Cr(VI) can be improved by increasing soil moisture.

3.3.2. Cr percentage in soil and the magnetic composite after separation

Since mineral composites have magnetic properties, soil remediation (50% water ratio and mineral dosage 20%) can be accomplished through the easy and efficient separation of soil from magnetic minerals using an external magnetic field. The percentage of Cr in soil and the magnetic composites was analyzed, with the results being shown in Fig. 5. In the control group, 63.8% of Cr can be leached by TCLP in the untreated soil, which means that about 60% of Cr is susceptible to migration. After treatment, only 3.6% of Cr is leached in the soil, indicating that a large amount of Cr is converted to stable phases through treating contaminated soil with magnetic minerals. Furthermore, we compared the percentage of Cr present in separated soil and magnetic minerals and found up to 58.2% of Cr was enriched in magnetic minerals. Under these

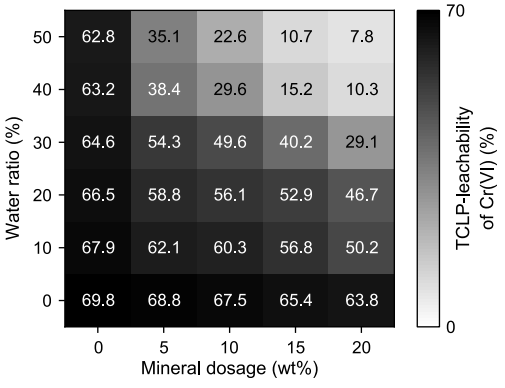

Fig. 4. The TCLP leachability of Cr(VI) under different water ratios and dosages of composites.

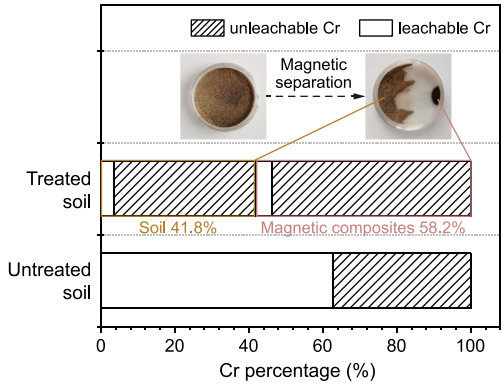

Fig. 5. Cr percentage in soils and the magnetic composite.

experimental conditions, the magnetic composites can adsorb mobile Cr from the soil for transportation to the surfaces, allowing its mineralization into more stable phases. Therefore, it is important to characterize the phase of these Cr-containing products that are enriched on the surface of the composites.

3.4. Characterization of the Cr(VI) products on the magnetic composite

The Cr-loaded composites particles formed after Cr reduction in the soil were characterized using SEM-EDS, Raman techniques, and XPS. The results shown in Fig. 5 demonstrate that *in-situ* remediation significantly reduces the amount of leachable Cr(VI) in the soil. This indicates that Cr(VI) was converted to an insoluble solid phase. The image of SEM (Fig. 6a) shows that a large number of new flocculent mineral phases were attached to the surface of the composites after the occurrence of the reaction. The mapping of EDS (Fig. 6a) shows that the Cr distribution is consistent with these newly formed minerals. Unattached Cr-bearing minerals on the surface of particles were dominated by S, and none of the Fe and O were enriched.

To further confirm the mechanism of the Cr(VI) reduction process and specify possible Cr species present on the surface, Raman spectroscopy was applied to the same sample. Results are shown in Fig. 6b. The new solid phases attached to the surface of pyrrhotite particles have several new peaks. Wang et al. [61] found that Raman peaks for Hematite were located at 227, 292, 411, 497, and 1319 cm^{-1}. In the present study, it was found that the new products have Raman peaks at 220, 286, 405, 492, and 1312 cm^{-1}; these peaks shifted positions to the left compared with those reported in similar literature. This shift may be due to the unique phase of Cr(III), or chromite, present within the crystal lattice [61]. Predecessors pointed out in the literature that the Raman spectral pattern of chromite consists of a major broad peak near 685 cm^{-1} and a shoulder near 650 cm^{-1} [62,63]. Thus, the peak near 686 cm^{-1} in Fig. 6b is consistent with the peaks for chromite in solid products.

Element valence and chemical oxidation states of surface and near-surface species of chromite were investigated using XPS. All spectra were drawn and analyzed using the Casa-XPS software [38]. The Cr 2p spectrum of the Cr-bearing minerals can be divided into three individual component peaks, which originated from the Cr(III) atom and overlap with each other. According to Moulder et al. [64], the Cr 2p peak for Cr oxides occurs at binding energy ranges of 575–580 eV. As shown in Fig. 6b, the peaks at binding energies of 577.5, 577.0, 575.9, and 575.7 eV can be assigned to Cr(III) species, indicating its complete reduction. Biesinger et al. [65] observed that $FeCr_2O_4$ peaks are found at binding energies of 575.9, 577.0, and 577.9 eV. Lastly, Pratt et al. [66] revealed that the Cr_2O_3 peak is found at binding energies of 575.7 eV, and the peak found at binding energies of 577.5 eV belongs to $Cr(OH)_3$. The theoretical mass proportion of $FeCr_2O_4$ is about 54.9%, 30.9% for $Cr(OH)_3$, and 14.2% for Cr_2O_3. These results are consistent with the element mapping and Raman data.

Based on SEM-EDS, Raman, and XPS data, it can be found that Cr(VI) in the soil is effectively reduced and immobilized; it is further mineralized on the surface of the composites in the form of $Cr(OH)_3$, Cr_2O_3, and $FeCr_2O_4$.

3.5. The mechanism of remediation

Combined with the experimental results of this paper and previous literature [67,68], we can infer that the mechanism of remediation of Cr(VI) contaminated soil by the magnetic mineral composites should include: Cr(VI) in the contaminated soil is dissolved in aqueous solution and exists in soil solution as $Cr_2O_7^{2-}$. Under the acidic condition, the surface of the mineral composite is positively charged, and the $Cr_2O_7^{2-}$ in the soil solution is preadsorbed on the surface of the magnetic composite under electrostatic action. Fe(II) and S(II) on the surface of mineral composites transfer electrons to Cr(VI) in the following ways:

$$6Fe(II) + Cr_2O_7^{2-} + 14H^+ \rightarrow 2Cr(III) + 6Fe(III) + 7H_2O$$

$$3S(II) + Cr_2O_7^{2-} + 14H^+ \rightarrow 2Cr(III) + 3S + 7H_2O$$

Cr(III) co-precipitates with Fe(II) and Fe(III) on the mineral surface, forming minerals and covering the surface of composite particles.

$$Cr(III) + Fe(III) + 3OH^- \rightarrow (Fe,Cr)(OH)_3$$

$$2Cr(III) + Fe(II) + 8OH^- \rightarrow FeCr_2O_4 + 4\ H_2O$$

$$2Cr(III) + 6OH^- \rightarrow Cr_2O_3 + 3H_2O$$

Under the external magnetic field, the Cr-containing products are separated from the soil along with the magnetic composites, so as to completely reduce the content of Cr in the soil and fundamentally solve the problem of Cr re-oxidized after the remediation.

4. Conclusion

In summary, we found a natural mineral composite consisting of 77% magnetite and 23% pyrrhotite with strong magnetic properties. Magnetite and pyrrhotite in the mineral composites are interlaced and closely bonded. XRF results show the absence of other heavy

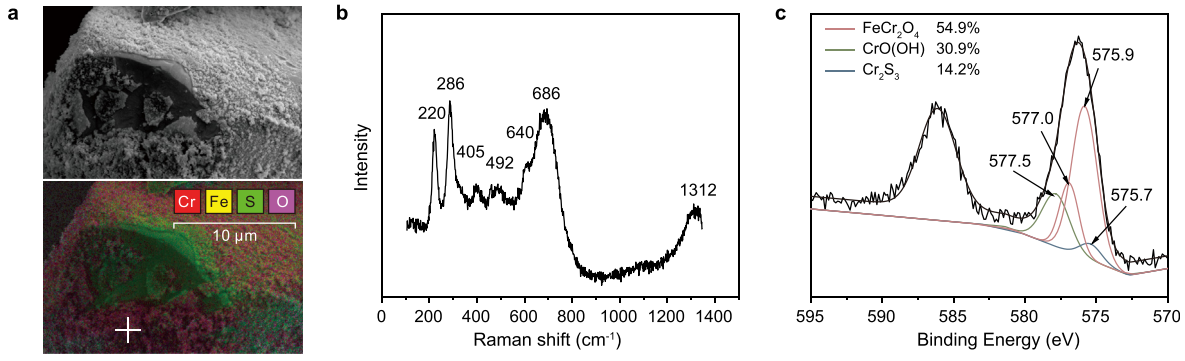

Fig. 6. **a**, SEM-EDS mapping image of the magnetic composite after the reaction. **b**, The Raman spectra of products. **c**, The XPS spectra of Cr 2p.

metals. Aqueous Cr removal experiments exhibit the significant immobilization effect of the composites on Cr(VI). This immobilization effect increases inversely with composite particle size. When the particle size is less than 150 μm, this allows for higher exposure of pyrrhotite surface area. The removal of Cr(VI) by the composite occurs through chemical adsorption. Acidic conditions are more favorable for the immobilization of Cr(VI). In this study, when the pH was 2, the amount of Cr(VI) removal per gram of composite was 45.8 mg g^{-1}. After 100 days of composite *in-situ* remediation, the leaching concentration (TCLP) of Cr(VI)-contaminated soil was 1.95 mg L^{-1}. After remediation, composites were separated from the soil by a magnetic field, and 58.2% of Cr was enriched through magnetic minerals. It was found that Cr was enriched on the surface of the composites in the form of $Cr(OH)_3$, Cr_2O_3, and $FeCr_2O_4$. Therefore, we concluded that *in-situ* reduction and mineralization of Cr(VI) in the soil could be carried out effectively by natural magnetic mineral composites and easily separated and removed from contaminated soil. This offers a novel approach to achieving clean remediation of soil contaminated by Cr(VI) and other hazardous oxyanions such as uranium.

Declaration of competing interest

The authors declare that they have no known competing financial interests or personal relationships that could have appeared to influence the work reported in this paper.

Acknowledgment

This work was supported by the National KeyResearch and Development Project of China [2019YFC1805900].

References

[1] Sun, et al., Removal of chromium from a contaminated soil using oxalic acid, citric acid, and hydrochloric acid: dynamics, mechanisms, and concomitant removal of non-targeted metals, Int. J. Environ. Res. Publ. Health 16 (15) (2019) 2771.
[2] R. Jobby, et al., Biosorption and biotransformation of hexavalent chromium [Cr(VI)]: a comprehensive review, Chemosphere 207 (2018) 255–266.
[3] P.M. Fernández, et al., Bioremediation strategies for chromium removal: current research, scale-up approach and future perspectives, Chemosphere 208 (2018) 139–148.
[4] Y. Li, et al., Remediation of hexavalent chromium spiked soil by using synthesized iron sulfide particles, Chemosphere 169 (2017) 131–138.
[5] B. Saha, C. Orvig, Biosorbents for hexavalent chromium elimination from industrial and municipal effluents, Coord. Chem. Rev. 254 (23–24) (2010) 2959–2972.
[6] S.J. Yu, et al., Recent Advances in Metal-Organic Framework Membranes for Water Treatment: A Review, Science of the Total Environment, 2021, p. 800.
[7] N.V. Mandich, Chemistry & theory of chromium deposition .1. Chemistry, Plat. Surf. Finish. 84 (5) (1997) 108–115.
[8] S.A. Katz, H. Salem, The toxicology of chromium with respect to its chemical speciation: a review, J. Appl. Toxicol. 13 (3) (1993) 217–224.
[9] M. Race, et al., Assessment of optimal conditions for the restoration and recovery of agricultural soil, J. Hazard Mater. 373 (2019) 801–809.
[10] J. Qian, et al., Direct Cr (VI) bio-reduction with organics as electron donor by anaerobic sludge, Chem. Eng. J. 309 (2017) 330–338.
[11] S. Mandal, et al., Enhancement of chromate reduction in soils by surface modified biochar, J. Environ. Manag. 186 (2017) 277–284.
[12] H.G. Gorchev, G. Ozolins, Who guidelines for drinking-water quality, WHO Chron. 38 (3) (1984) 104–108.
[13] A.U. Rajapaksha, et al., Removal of hexavalent chromium in aqueous solutions using biochar: chemical and spectroscopic investigations, Sci. Total Environ. 625 (2018) 1567–1573.
[14] O. Husson, Redox potential (Eh) and pH as drivers of soil/plant/microorganism systems: a transdisciplinary overview pointing to integrative opportunities for agronomy, Plant Soil 362 (1–2) (2013) 389–417.
[15] T.E. Higgins, A.R. Halloran, J.C. Petura, Traditional and innovative treatment methods for Cr(VI) in soil, J. Soil Contam. 6 (6) (1997) 767–797.
[16] K.R. Reddy, et al., Effects of soil composition on the removal of chromium by electrokinetics, J. Hazard Mater. 55 (1–3) (1997) 135–158.
[17] W. Zhang, et al., Influence of EDTA washing on the species and mobility of heavy metals residual in soils, J. Hazard Mater. 173 (1–3) (2010) 369–376.
[18] C.M. Lytle, et al., Reduction of Cr(VI) to Cr(III) by wetland plants: potential for in situ heavy metal detoxification, Environ. Sci. Technol. 32 (20) (1998) 3087–3093.
[19] H. Su, et al., Stabilisation of nanoscale zero-valent iron with biochar for enhanced transport and in-situ remediation of hexavalent chromium in soil, Environ. Pollut. 214 (2016) 94–100.
[20] H. Lyu, et al., Immobilization of hexavalent chromium in contaminated soils using biochar supported nanoscale iron sulfide composite, Chemosphere 194 (2018) 360–369.
[21] L. Alidokht, et al., Cr(VI) immobilization process in a Cr-spiked soil by zerovalent iron nanoparticles: optimization using response surface methodology, Clean 39 (7) (2011) 633–640.
[22] B. Eyvazi, A. Jamshidi-Zanjani, A. Khodadadi Darban, Immobilization of hexavalent chromium in contaminated soil using nano-magnetic MnFe2O4, J. Hazard Mater. 365 (2019) 813–819.
[23] A. Reyhanitabar, et al., Application of stabilized Fe0nanoparticles for remediation of Cr(VI)-spiked soil, Eur. J. Soil Sci. 63 (5) (2012) 724–732.
[24] Y. Gong, J. Tang, D. Zhao, Application of iron sulfide particles for groundwater and soil remediation: a review, Water Res. 89 (2016) 309–320.
[25] Y. Li, et al., Reduction and immobilization of hexavalent chromium in chromite ore processing residue using amorphous FeS2, Sci. Total Environ. 658 (2019) 315–323.
[26] S.J. Yu, et al., MXenes as Emerging Nanomaterials in Water Purification and Environmental Remediation, Science of the Total Environment, 2022, p. 811.
[27] B.W. Hu, et al., Efficient elimination of organic and inorganic pollutants by biochar and biochar-based materials, Biochar 2 (1) (2020) 47–64.
[28] N. Zhang, Z. Fang, R. Zhang, Comparison of several Amendments for in-site remediating chromium-contaminated farmland soil, Water air Soil Pollut. 228 (10) (2017).
[29] K.D. Grieger, et al., Environmental benefits and risks of zero-valent iron nanoparticles (nZVI) for in situ remediation: risk mitigation or trade-off? J. Contam. Hydrol. 118 (3–4) (2010) 165–183.
[30] M. Stefaniuk, P. Oleszczuk, Y.S. Ok, Review on nano zerovalent iron (nZVI): from synthesis to environmental applications, Chem. Eng. J. 287 (2016) 618–632.
[31] N. Belzile, et al., A review on pyrrhotite oxidation, J. Geochem. Explor. 84 (2) (2004) 65–76.
[32] H. Wang, A review on process-related characteristics of pyrrhotite, Miner. Process. Extr. Metall. Rev. 29 (1) (2007) 1–41.
[33] A. Lu, et al., Removal of Cr(VI) and Cr(lll) from aqueous solutions and industrial wastewaters by natural clino-pyrrhotite, Environ. Sci. Technol. 40 (9) (2006) 3064–3069.
[34] S.A. Baig, et al., Hexavalent chromium removal from solutions: surface efficacy and characterizations of three iron containing minerals, Clean 42 (10) (2014) 1409–1414.
[35] J. Sphar, Occurrence of magnetite in the Arkansas river bed between ford and Arkansas city, Trans. Kans. Acad. Sci. 65 (3) (1962) 257, 1903-.
[36] B.A. Maher, R.M. Taylor, Formation of ultrafine-grained magnetite in soils, Nature 336 (6197) (1988) 368–370.
[37] J. Chang, et al., New insight into adsorption and reduction of hexavalent chromium by magnetite: multi-step reaction mechanism and kinetic model developing, Colloids Surf. A Physicochem. Eng. Asp. 611 (2021) 125784.
[38] S.R. Chowdhury, E.K. Yanful, A.R. Pratt, Chemical states in XPS and Raman analysis during removal of Cr(VI) from contaminated water by mixed maghemite-magnetite nanoparticles, J. Hazard Mater. 235–236 (2012) 246–256.
[39] S. Yang, et al., Ultrahigh sorption and reduction of Cr(VI) by two novel core-shell composites combined with Fe3O4 and MoS2, J. Hazard Mater. 379 (2019) 120797.
[40] W. Shen, et al., Magnetic Fe3O4–FeB nanocomposites with promoted Cr(VI) removal performance, Chem. Eng. J. 285 (2016) 57–68.
[41] W. Jiang, et al., Cr(VI) adsorption and reduction by humic acid coated on magnetite, Environ. Sci. Technol. 48 (14) (2014) 8078–8085.
[42] Y. Wang, et al., Remediation of hexavalent chromium contaminated soil by stabilized nanoscale zero-valent iron prepared from steel pickling waste liquor, Chem. Eng. J. 247 (2014) 283–290.
[43] J. Zhong, et al., Column study of enhanced Cr(VI) removal and longevity by coupled abiotic and biotic processes using Fe(0) and mixed anaerobic culture, Water Res. 122 (2017) 536–544.
[44] Y. Wang, et al., Immobilization and phytotoxicity of chromium in contaminated soil remediated by CMC-stabilized nZVI, J. Hazard Mater. 275 (2014) 230–237.
[45] J. Du, et al., Reduction and immobilization of chromate in chromite ore processing residue with nanoscale zero-valent iron, J. Hazard Mater. 215–216 (2012) 152–158.
[46] W.-J. Zhang, M.-F. Lin, Influence of redox potential on leaching behavior of a solidified chromium contaminated soil, Sci. Total Environ. 733 (2020) 139410.
[47] H. Tan, et al., Remediation of hexavalent chromium contaminated soil by nano-FeS coated humic acid complex in combination with Cr-resistant microflora, Chemosphere 242 (2020) 125251.
[48] Z. Jalil, et al., Magnetic Behavior of Natural Magnetite (Fe3O4) Extracted from Beach Sand Obtained by Mechanical Alloying Method, 2017.
[49] Y. Liao, et al., Recyclable naturally derived magnetic pyrrhotite for elemental mercury recovery from flue gas, Environ. Sci. Technol. 50 (19) (2016) 10562–10569.

[50] G. Ren, et al., Chromium (VI) adsorption from wastewater using porous magnetite nanoparticles prepared from titanium residue by a novel solid-phase reduction method, Sci. Total Environ. 607–608 (2017) 900–910.
[51] M.L. Rivas-Sánchez, et al., Natural magnetite nanoparticles from an iron-ore deposit: size dependence on magnetic properties, Earth Planets Space 61 (1) (2009) 151–160.
[52] O.N. Shebanova, P. Lazor, Raman spectroscopic study of magnetite (FeFe2O4): a new assignment for the vibrational spectrum, J. Solid State Chem. 174 (2) (2003) 424–430.
[53] P. Ruiz-Galende, et al., Study of a terrestrial Martian analogue: geochemical characterization of the Meñakoz outcrops (Biscay, Spain), J. Raman Spectrosc. 51 (9) (2020) 1603–1612.
[54] T. Pasinszki, et al., Carbon microspheres decorated with iron sulfide nanoparticles for mercury(II) removal from water, J. Mater. Sci. 55 (4) (2020) 1425–1435.
[55] M.J. Dekkers, M.A.A. Schoonen, An electrokinetic study of synthetic greigite and pyrrhotite, Geochem. Cosmochim. Acta 58 (19) (1994) 4147–4153.
[56] P.H. Tewari, A.B. Campbell, Dissolution of iron sulfide (troilite) in aqueous sulfuric acid, J. Phys. Chem. 80 (17) (1976) 1844–1848.
[57] Y. Xu, D. Zhao, Reductive immobilization of chromate in water and soil using stabilized iron nanoparticles, Water Res. 41 (10) (2007) 2101–2108.
[58] Y.P. Liao, et al., Migration and transfer of chromium in soil-vegetable system and associated health risks in vicinity of ferro-alloy manufactory, Trans. Nonferrous Metals Soc. China 21 (11) (2011) 2520–2527.
[59] D.A. Sverjensky, Zero-Point-of-Charge prediction from crystal-chemistry and solvation theory, Geochem. Cosmochim. Acta 58 (14) (1994) 3123–3129.
[60] H. Strandh, et al., Quantum chemical studies of the effects on silicate mineral dissolution rates by adsorption of alkali metals, Geochem. Cosmochim. Acta 61 (13) (1997) 2577–2587.
[61] A. Wang, et al., Raman spectroscopy of Fe-Ti-Cr-oxides, case study: Martian meteorite EETA79001, Am. Mineral. 89 (5–6) (2004) 665–680.
[62] V. D'Ippolito, et al., Raman fingerprint of chromate, aluminate and ferrite spinels, J. Raman Spectrosc. 46 (12) (2015) 1255–1264.
[63] D. Lenaz, V. Lughi, Raman study of MgCr2O4–Fe2+Cr2O4 and MgCr2O4–MgFe2 3+O4 synthetic series: the effects of Fe2+ and Fe3+ on Raman shifts, Phys. Chem. Miner. 40 (6) (2013) 491–498.
[64] J.F. Moulder, et al., Handbook of X-Ray Photoelectron Spectroscop, 1992.
[65] M.C. Biesinger, et al., Resolving surface chemical states in XPS analysis of first row transition metals, oxides and hydroxides: Cr, Mn, Fe, Co and Ni, Appl. Surf. Sci. 257 (7) (2011) 2717–2730.
[66] A.R. Pratt, N.S. McIntyre, Curve fitting of Cr 2p photoelectron spectra of Cr2O3 and CrF3 - Comment, Surf. Interface Anal. 24 (8) (1996) 529–530.
[67] F.L. Liu, et al., Insight into the performance and mechanism of persimmon tannin functionalized waste paper for U(VI) and Cr(VI) removal, Chemosphere (2022) 287.
[68] F.L. Liu, et al., Adsorption and reduction of Cr(VI) from aqueous solution using cost-effective caffeic acid functionalized corn starch, Chemosphere (2021) 279.